# Fragments and dust after Holmium laser lithotripsy with or without "Moses technology": How are they different?

Etienne X. Keller, Vincent de Coninck, Marie Audouin, Steeve Doizi, Dominique Bazin, Michel Daudon, Olivier Traxer

▶ **To cite this version:**

HAL Id: hal-02160945

https://hal.sorbonne-universite.fr/hal-02160945v1

Submitted on 20 Jun 2019

Journal of
BIOPHOTONICS

**FULL ARTICLE**

# Fragments and dust after Holmium laser lithotripsy with or without "Moses technology": How are they different?

Etienne X. Keller[1,2,3] | Vincent de Coninck[1,2,4] | Marie Audouin[1,2] | Steeve Doizi[1,2] | Dominique Bazin[5,6] | Michel Daudon[7,8,9] | Olivier Traxer[1,2]*

[1]Service d'Urologie, Sorbonne Université, Service d'Urologie, AP-HP, Hôpital Tenon, Paris, France

[2]Groupe de Recherche Clinique sur la Lithiase Urinaire, Sorbonne Université, GRC no 20, Groupe de Recherche Clinique sur la Lithiase Urinaire, Hôpital Tenon, Paris, France

[3]Department of Urology, University Hospital Zurich, University of Zurich, Zurich, Switzerland

[4]Department of Urology, AZ Klina, Brasschaat, Belgium
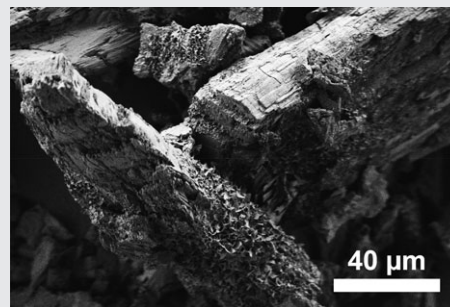
[5]CNRS, Laboratoire de Chimie de la Matière Condensée de Paris, UPMC, Collège de France, Paris, France

[6]Laboratoire de Physique des Solides, CNRS UMR 8502, Université Paris Sud XI, Orsay, France

[7]CRISTAL Laboratory, Tenon Hospital, Paris, France

[8]Laboratoire des Lithiases, Service des Explorations Fonctionnelles Multidisciplinaires, AP-HP, Hôpital Tenon, Paris, France

[9]UMRS 1155 UPMC, INSERM, UMRS 1155 UPMC, Tenon Hospital, Paris, France

**\*Correspondence**
Olivier Traxer, Service d'Urologie, Hôpital Tenon, Assistance-Publique Hôpitaux de Paris, 4 rue de la Chine, 75020 Paris, France.
Email: olivier.traxer@aphp.fr

Urinary stones can be readily disintegrated by Holmium:YAG laser (Holmium laser lithotripsy), resulting in a mixture of small stone dust particles, which will spontaneously evacuate with urine and larger residual fragments (RF) requiring mechanical retrieval. Differences between fragments and dust have not been well characterized. Also, it remains unknown how the recently introduced "Moses technology" may alter stone disintegration products. Three complementary analytical techniques have been used in this study to offer an in-depth characterization of disintegration products after in vitro Holmium laser lithotripsy: stereoscopic microscopy, scanning electron microscopy and Fourier-transform infrared spectroscopy. Dust was separated from fragments based on its floating ability in saline irrigation. Depending on initial crystalline constituents, stone dust either conserved attributes found in larger RFs or showed changes in crystalline organization. These included conversion of calcium oxalate dihydrate towards calcium oxalate monohydrate, changes in carbapatite spectra towards an amorphous phase, changes of magnesium ammonium phosphate towards a differing amorphous and crystalline phase and the appearance of hydroxyapatite on brushite fragments. Comparatively, "Moses technology" produced more pronounced changes. These findings provide new insights suggesting a photothermal effect occurring in Holmium laser lithotripsy. Figure: Appearance of hydroxyapatite hexagons on stone dust collected after Holmium laser lithotripsy of a brushite stone using "Moses technology."

**KEYWORDS**
Fourier-transform infrared spectroscopy, holmium laser, lithotripsy, Moses effect, residual fragments, scanning electron microscopy, stone dust, urinary stone

## 1 | INTRODUCTION

Over the past two decades, Holmium:YAG laser (thereafter referred as Holmium laser) has become a readily

available energy source for endourologic procedures allowing lithotripsy of all known urinary stone types [1]. Holmium laser operates at a wavelength of 2120 nm—near to the 1940 nm water absorption peak [2]—and transmits pulsed energy (pulse duration ≥250 μs)

Etienne X. Keller and Vincent de Coninck contributed equally to this study.

www.biophotonics-journal.org

through thin silica fibers. The true effect of Holmium laser on stones has been the object of an ongoing debate. A photothermal effect is believed to be the primary mechanism leading to fragmentation during Holmium laser lithotripsy [3, 4]. Contrarily, the formerly used pulsed dye laser (pulse duration ~1 μs) and Neodymium:YAG laser (pulse duration ~0.5 μs) had been shown to accomplish lithotripsy by a photoacoustical mechanism (plasma expansion and cavitation collapse), a characteristic that was not found for Holmium laser lithotripsy [3, 5].

Delivery of Holmium laser energy on stones has been proposed to be most effective with the occurrence of the "Moses effect" in water. This phenomenon was first described in 1988 and relies on the vaporization of water by laser energy, such that the successive portion of the laser pulse transmits through vapor instead of water [6]. This allows for an enhanced transmission of the laser energy to the target stone. The recently developed "Moses technology" therefore uses pulse modulation to deliver a considerable fraction of total pulse energy through the vapor channel for ideal energy delivery [7].

Stone disintegration products from Holmium lithotripsy generally form a mixture of larger residual fragments (RF) and smaller stone dust particles [8, 9]. Growing enthusiasm for laser dusting techniques has emerged over the last years, owing to the observation that dust particles seem to have a propensity for spontaneous evacuation from kidney after ureteroscopic laser lithotripsy, omitting the need for time-consuming fragment extraction [10]. A previous study demonstrated the feasibility of stone dust aspiration through the working channel of flexible ureteroscopes (fURS) [11]. Nevertheless, a clear definition of stone dust has not been established yet. Also, it is not known whether alterations of the initial crystalline constitution may be found after Holmium lithotripsy and whether "Moses technology" may produce differing stone disintegration products. It is thus necessary to further characterize RF and stone dust to help understand the true effect of Holmium laser on stones.

The present study offers an in-depth morpho-constitutional analysis of the disintegration products from Holmium lithotripsy for the seven most frequently encountered crystalline constituents of urinary stones.

## 2 | MATERIALS AND METHODS

Urinary stones were retrieved from a large stone biobank that was built over the last 33 years at our institution. Crystalline constituents analyzed in this study were: calcium oxalate monohydrate (COM), calcium oxalate dihydrate (COD), uric acid (UA), carbapatite (carbonated calcium phosphate; CA), struvite (magnesium ammonium phosphate; MAP), brushite (BR) and cystine (CYS). Criteria for stone selection

were size >1000 mm$^3$ and >90% pure stone composition. The later was based on a detailed morpho-constitutional analysis of stones' surface, section and core, including Fourier-transform infrared (FTIR) spectroscopic analysis for each single stone available in the stone biobank, as previously described [12]. Inappropriate stone storage (eg, wet storage conditions, missing or altered box labeling) was an exclusion criterion. The study was in accordance with ethical standards of the Helsinki declaration.

### 2.1 | Sample preparation

Each stone was cut with a surgical knife into pieces of ~300 mm$^3$, which were immersed in sterile saline solution (0.9%) for 24 hours. Laser lithotripsy was then performed with a Lumenis P120H Holmium laser generator (Lumenis Ltd., Yokneam, Israel). A dusting setting (0.2 J, 40 Hz, long pulse, Lumenis SlimLine D/F/L 200 μm fibers) was compared to the Moses mode (0.2 J, 40 Hz, Moses "contact" mode, MOSES SlimLine 200 μm fibers), thereafter referred as Moses lithotripsy [13, 14]. Laser fibers were inserted into a Lithovue fURS (Boston Scientific, Maple Grove, Minnesota) and laser lithotripsy was performed under direct visual control in a 5.8 mL glass container (inner diameter 10 mm, height 74 mm) using sterile saline irrigation at room temperature with an irrigation pressure of 40 cm H20 (Figure 1-A), until a total of 2400 J were delivered. Lithotripsy was performed free-hand with painting movements of laser fiber tip over stone samples. Laser fiber tips were cut with normal scissors before lithotripsy of each sample. The irrigation overflow was collected in a 100 mL plastic container.

After laser lithotripsy, larger RF were separated from stone dust using a method based on the floating ability of particles. For this, the content of the glass container comprising a mixture of RF and dust was poured into a 60 mL plastic container, which was perforated with a hole located 2 cm above the bottom of the container (Figure 1-B). This allowed for dust particles with floating ability to evacuate through the hole when a constant irrigation through the f-URS was applied (empty working channel, irrigation pressure of 40 cm H20). The size of the hole (5 mm) was chosen to allow sufficient irrigation outflow from the plastic container. The resulting irrigation overflow was collected in the same 100 mL plastic container that was used during lithotripsy (Figure 1-C). The RF without floating ability remained within the 60 mL plastic container and stone dust from the 100 mL was allowed to sediment under terrestrial gravity.

### 2.2 | Morphological analysis

For morphological analysis, each air-dried RF or dust sample was separately transferred on carbon conductive double-faced adhesive tapes (Nisshin EM Co. Ltd., Tokyo, Japan). Images were obtained from an Olympus SZ61 stereoscopic microscope (Olympus Corporation, Tokyo, Japan), as well

as from a Zeiss Gemini Supra 55VP scanning electron microscope (SEM) (Carl Zeiss AG, Oberkochen, Germany) using low electron beam voltage ($\leq 2$ keV) [15]. For each sample, three different areas of interest were analyzed by SEM. No sample coating or fixation was needed for these analyses. Morphological stone types were classified according to the Daudon classification of stones [16, 17].

## 2.3 | Constitutional analysis

FTIR spectroscopy was used to identify chemical constituents of each sample, as described previously [18]. Sample preparation included fine grinding of RF or dust, respectively, together with a purified salt (potassium bromide) and applying 10 tons to this mixture with a mechanical press to form a translucent pellet, which was placed into a Bruker Vector 22 spectrometer for analysis (Bruker Daltonik GmbH, Bremen, Germany). The density of a given RF or dust sample in its according pellet was limited to a level that generated spectral bands with a maximal intensity of 2.00 absorbance units in order to avoid scattering artifacts of intense bands. The FTIR spectra of the initial stones were compared to the spectra drawn from RF and dust samples.

## 3 | RESULTS

From >80 000 urinary stones listed in the biobank, one stone of each constitutional type was available for analysis. Table 1 summarizes patients' characteristics from whom stones were retrieved. Major constituent was >90% for each constitutional type, except for COD, CA and BR where a mixed stone of 85% COD, 87% CA and 85% BR had to be

selected, respectively, in order to align with the stone size requirements.

## 3.1 | Morphological analysis

Observations from morphological analyses are summarized in Table 2 and illustrated in Figures 2, 3 and 4. While only a few stone characteristics could be retrieved from stereoscopic microscopy (mainly color), the addition of SEM imagery allowed for an in-depth morphological analysis. For COM, the brown dust was characterized as small plates that kept a layered organization also found in larger RF. For COD, a bipyramidal organization was partially conserved in RF, whereas dust lost this attribute and merely conserved the initial beige-brown color within a heterogenous mixture of sharp particles. This was in contrast to UA, where both RF and dust revealed a partially conserved crystalline organization with smoother edges and brown-orange color. The surface of CA was a mixture of smooth and bumpy surfaces both in RF and dust samples. The MAP samples revealed longitudinal white needles which seemed to be encased in another constituent, an observation found both in RF and dust. For BR, the typical longitudinal organization was found in RF and was teared down to sharp and thin beige baguettes in dust samples. Finally, a layered organization of hexagons was found in RF and dust samples of CYS.

Peculiar observations emerged from comparison of conventional Holmium with Moses lithotripsy. Moses lithotripsy produced a more pronounced disruption of morphological characteristics of COD, MAP and CYS stones (Table 2). Also, areas with hexagonal plate-like surfaces appeared on RF and dust from BR after Moses lithotripsy (Figure 4). This plate-like morphology is

**TABLE 1** Patient characteristics for each constitutional stone type

| Constitutional stone type | COM | COD | UA | CA | MAP | BR | CYS |
|---|---|---|---|---|---|---|---|
| Gender | Male | Male | Female | Female | Male | Male | Female |
| Year of retrieval | 2001 | 2014 | 2017 | 1994 | 2008 | 2013 | 2001 |
| Age at retrieval, year. | 70 | 52 | 54 | 36 | 8 | 64 | 11 |
| Localization | Kidney | Kidney | Kidney | Kidney | Bladder | Bladder | Kidney |
| Associated urinary path abnormality | Uretero-pelvic junction obstruction | None | None | Medullary sponge kidney | Neuropathic bladder | Benign prostatic hyperplasia | None |
| Concomitant urinary infection | No | No | No | Yes, Proteus | Yes, urease-positive bacteria | No | No |
| Stone size, mm | 17 × 15 × 11 | 16 × 14 × 10 | 20 × 14 × 14 | 15 × 13 × 10 | 24 × 4 × 22 | 16 × 13 × 10 | 19 × 15 × 13 |
| Morphological stone type[a] | Id | IIb | IIIb | IVa1 | IVc | IVd | Va |
| Stone composition from initial FTIR analysis | 98% COM 1% UA 1% CA | 85% COD 8% COM 4% CA 3% Prot. | 100% anhydrous UA | 87% CA 6% PAM 5% COD 2% Prot. | 90% MAP 5% CA 3% Prot. 2% COM | 85% BR 5% COD 4% CA 3% COM 3% Prot. | 98% CYS 2% CA |

Abbreviations: BR, brushite; CA, carbapatite; COD, calcium oxalate dihydrate; COM, calcium oxalate monohydrate; CYS, cystine; MAP, magnesium ammonium phosphate; Prot., protein; UA, uric acid.
[a] According to the Daudon classification of stones [13].

**TABLE 2** Morphological characteristics for each constitutional stone type

| Stone type | Fragment type | Morphological description | | Laser-related peculiarities |
|---|---|---|---|---|
| | | Stereoscopic microscopy | Scanning electron microscopy | |
| COM | RF | Form: lamellar and radiating organization. Plates with matt smooth surfaces<br><br>Color: homogenous, brown. | Form: lamellar organization. Plates with smooth surfaces and few cracks, partially covered by smaller plates | — |
| | Dust | Form: no visible organization<br><br>Color: homogenous, brown | Form: lamellar organization. Randomly shaped plates with <5 layers, sharp edges and smooth surfaces | |
| COD | RF | Form: blocks with glossy rough surfaces and blunt translucid bipyramids<br><br>Color: beige to yellow-brown. | Form: blocks with partially conserved smooth bipyramidal organization and other more disorganized rough areas. Many cracks | Moses: more pronounced damages to the crystalline organization |
| | Dust | Form: no visible organization<br><br>Color: heterogenous mixture of beige and yellow-brown particles | Form: randomly shaped particles with sharp edges and a mixture of smooth and rough surfaces. Loss of bipyramidal organization | |
| UA | RF | Form: blocks with glossy rough surfaces<br><br>Color: brown-orange | Form: blocks with rough surfaces consisting of rather conserved smooth crystals | — |
| | Dust | Form: no visible organization<br><br>Color: heterogenous mixture of brown and orange particles | Form: partially conserved crystalline organization with rather smooth edges and a mixture of smooth and rough surfaces. Few cracks | |
| CA | RF | Form: blocks with matt bumpy surfaces on a background of small round particles.<br><br>Color: beige blocks, white round particles | Form: blocks with partly smooth and partly granular surfaces, many cracks. The granular surface organization is due to small spherical compounds | — |
| | Dust | Form: no visible organization.<br><br>Color: homogenous white-beige. | Form: randomly shaped blocks with sharp edges and smooth to bumpy surfaces. Loss of spherical compounds | |
| MAP | RF | Form: blocks with glossy smooth surfaces on a background of sharp baguettes<br><br>Color: white | Form: blocks consisting of mono-directional longitudinal needles encased in a constituent forming an amalgam with many cracks | Moses: greater tendency to separate needles from their encasement |
| | Dust | Form: no visible organization<br><br>Color: homogenous white | Form: randomly configured needles encased in an amalgam | |
| BR | RF | Form: radial translucid glossy baguettes,<br><br>Color: translucid-white to yellow-brown | Form: entangled longitudinal baguettes with smooth or needle-like surfaces. Deep cracks | Moses: areas of hexagonal plate-like surfaces at the tip of a larger baguette (Figure 4), as well as on dust particles. |
| | Dust | Form: randomly overlapping baguettes<br><br>Color: white-beige. | Form: sharp and thin baguettes, few agglomerations of round particles | |
| CYS | RF | Form: blocks with glossy rough surfaces, visible layers, few areas of discernable hexagonal organization<br><br>Color: white-beige to yellow-brown | Form: blocks with a layered organization, smooth surfaces and recognizable hexagonal edges | Moses: many cracks and deep imprints. |
| | Dust | Form: glossy particles without visible organization<br><br>Color: homogenous, beige | Form: randomly shaped blocks with a layered organization, smooth surfaces and barely recognizable hexagonal edges | |

Abbreviations: BR, brushite; CA, carbapatite; COD, calcium oxalate dihydrate; COM, calcium oxalate monohydrate; CYS, cystine; MAP, magnesium ammonium phosphate; RF, residual fragments; UA, uric acid.

characteristic of hydroxyapatite formation and was not found in samples issued from conventional Holmium lithotripsy.

## 3.2 | Constitutional analysis

For COM, UA and CYS, the spectra of both RF and dust showed no changes when compared to their respective initial FTIR spectra. For COD, the characteristics bands at 1645 and 1324 $cm^{-1}$ remained unchanged in RF samples, whereas COD dust from conventional Holmium lithotripsy showed a tendency towards a conversion to COM. This was characterized by displacement of major bands at 1644 and 1323 $cm^{-1}$, as well as by the appearance of a prominent band at 781 $cm^{-1}$, which is characteristic for COM. The conversion from COD to COM became even more apparent in COD dust from Moses lithotripsy, with displaced major bands at 1628 and 1318 $cm^{-1}$, as well as a clearly identifiable band at 781 $cm^{-1}$ and the appearance of a discernable 662 $cm^{-1}$ band (Figure 5-A-B). RF of CA conserved all characteristics from their initial spectrum with prominent bands at 1035, 604 and 563 $cm^{-1}$, corresponding to phosphate absorption peaks. In contrast, CA dust from Moses
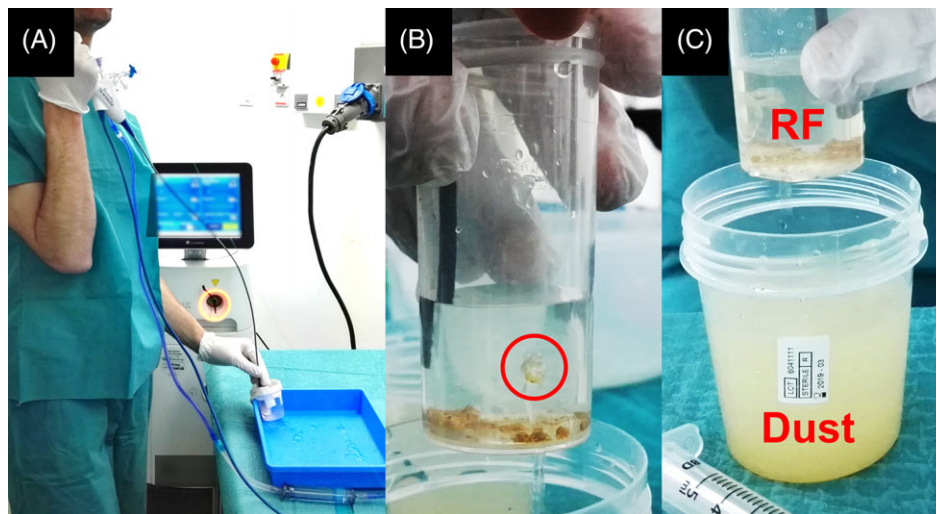
**FIGURE 1** Holmium laser lithotripsy and sample preparation. A, Laser lithotripsy performed under direct visual control with a Lumenis P120H Holmium laser generator, a 200 μm laser fiber and a Lithovue fURS. B, Separation of stone dust from RF using a method based on the floating ability of particles which can escape through a 5 mm hole drilled 2 cm from the bottom of the container (red circle). C, Separate collection of irrigation overflow containing dust particles

lithotripsy had a major band that moved towards 1038 cm$^{-1}$ with a flattened shape signing a change towards an amorphous phase (Figure 5C-D). Interestingly, this loss of crystalline phase allowed for the appearance of clearly distinguishable bands at 1315 and 781 cm$^{-1}$ in CA dust from Moses lithotripsy, thus, undercovering COM content in this sample. This COM arguably resulted from laser-induced conversion of the COD constituent that was present in the initial sample. MAP samples did not show any changes compared to their initial MAP spectrum, except for MAP dust from Moses lithotripsy where a profound loss of the ammonium bands at 1470 and 1435 cm$^{-1}$, a displacement of 1008 cm$^{-1}$ band towards 1084 cm$^{-1}$ and a loss of water content was found (Figure 5E-F). Finally, for BR, conventional Holmium lithotripsy did not change the spectrum of RF, whereas there was a heightening of the indentation between the 1063 and 987 cm$^{-1}$ bands in RF of BR after Moses lithotripsy, signing a higher proportion of apatite. The change from BR towards CA became even more evident on dust samples from both conventional Holmium and Moses lithotripsy, with the disappearance of a 987 and 661 cm$^{-1}$ band, a profound disturbance of the 1136 and 1063 cm$^{-1}$ bands, the appearance of 603 and 563 cm$^{-1}$ bands and loss of water content (Figure 5-G-H).

## 4 | DISCUSSION

To the best of our knowledge, the present study is the first of its kind providing a comprehensive morpho-constitutional analysis of disintegration products occurring during Holmium lithotripsy. The seven most frequently encountered stone types in our institution were analyzed [16]. Depending on major crystalline constituents, stone dust either conserved

all attributes found in larger RF or showed changes in the crystalline organization. Particularly, stone dust particles from COM, UA and CYS were found to have the same crystalline organization as in RF. In contrast, stone dust from COD, CA, MAP and BR showed fundamental morpho-constitutional changes. Of interest, changes seemed to be more pronounced in samples issued from Moses lithotripsy.

Schafer et al. proposed that stone melting and recrystallisation occurs during Holmium lithotripsy [19]. This hypothesis was based on the observation of filamentous stone particles at microscopy after Holmium lithotripsy of pigmented biliary stones. Such conclusions may not be valid for urinary stones based on the findings of the current study, because both RF and stone dust issued from COM, UA and CYS seemed to preserve all their morpho-constitutional characteristics. In line with these findings, a previous study involving SEM analysis of COM stones showed that lasered stone craters had a similar lamellar morphology found in non-ablated areas of stone fracture [20]. However, that study only analyzed stone craters, contrarily to the present report where stone fragments themselves were analyzed.

A previous matched-pair comparison of RF with stone dust showed 74% concordance in stone constituents, with intact FTIR spectra in all UA dust sample and complete loss of MAP spectra in all according to dust samples [11]. In line with those findings, UA dust indeed conserved morphological-constitutional characteristics of RF in the present study. As for MAP, a fundamentally novel characteristic was discovered by SEM analysis in both RF and dust samples, which revealed an organization of longitudinal white needles encased in another constituent. An according change of FTIR spectrum was found in MAP dust from Moses lithotripsy, which showed changes towards a differing amorphous and crystalline phase.
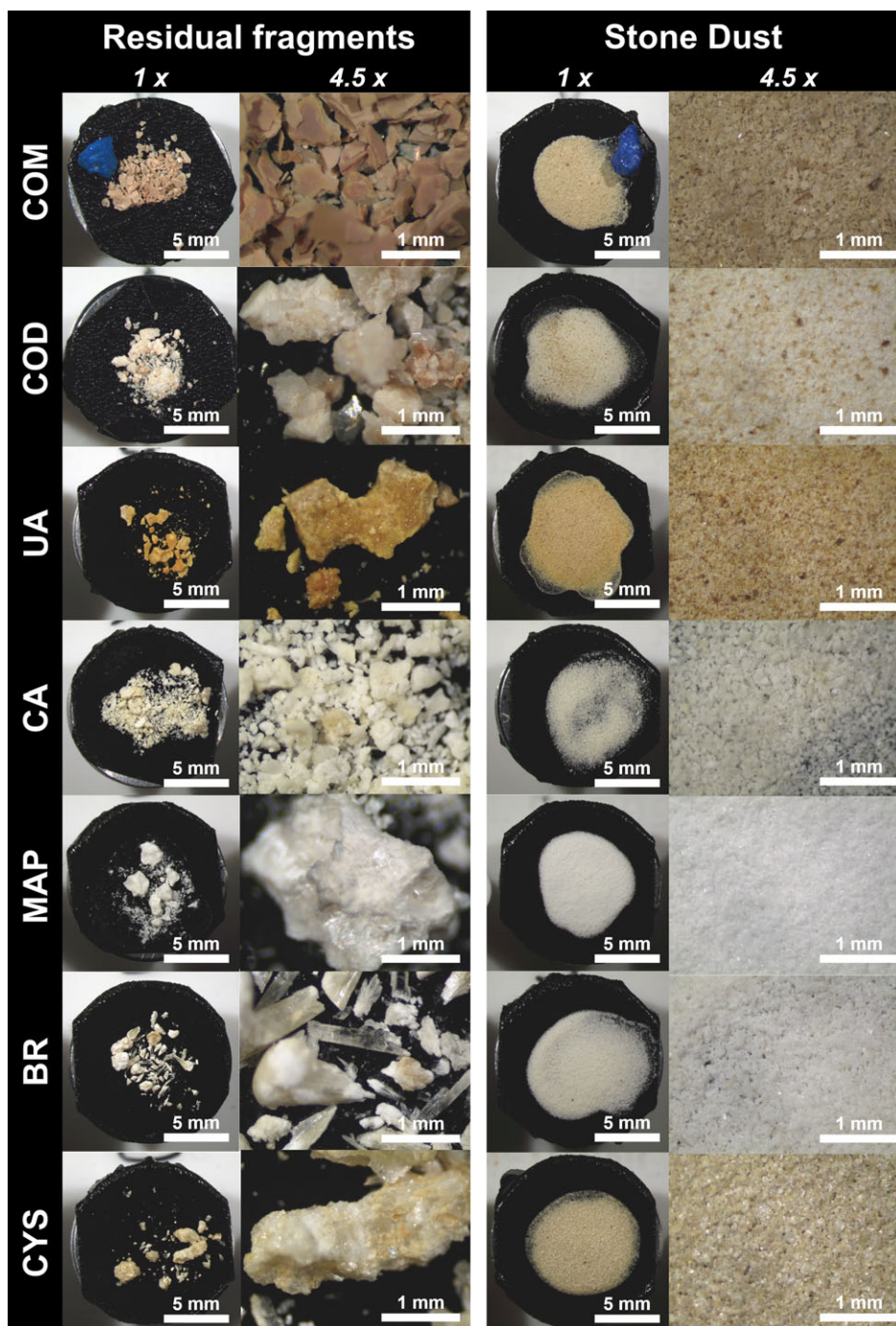
**FIGURE 2** Morphological analysis by stereoscopic microscopy. Each stone constituent was analyzed by stereoscopic microscopy at magnifications of 1× and 4.5×. Dried RF and stone dust were put on carbon conductive double-faced adhesive tapes to allowed subsequent morphological analysis by SEM. A blue plastic marker was placed on the COM samples for orientation purposes during sample positioning in the SEM machine

Several further peculiar observations such as the conversion of COD towards COM, changes in CA spectra towards an amorphous phase as well as the appearance of hydroxyapatite on BR fragments suggest that stones were subject to a direct photothermal effect from Holmium laser in this study. Considering that—at equivalent pulse energy—Moses technology may deliver superior laser beam through vapor channel compared to conventional Holmium laser, it may have been that higher local temperatures occurred during Moses lithotripsy. This would explain

why more pronounced morpho-constitutional changes were observed in Moses samples compared to conventional Holmium lithotripsy. The direct photothermal effect has been supported by prior chemical analyses which revealed thermal decomposition products after Holmium lithotripsy, including the appearance of hydroxyapatite in laser impact craters on BR stone surface, in line with the findings of the present study [3]. Other crystalline phase changes, such as COM to calcium carbonate, UA to cyanide, BR to CA, hydroxyapatite to calcium pyrophosphate, MAP to
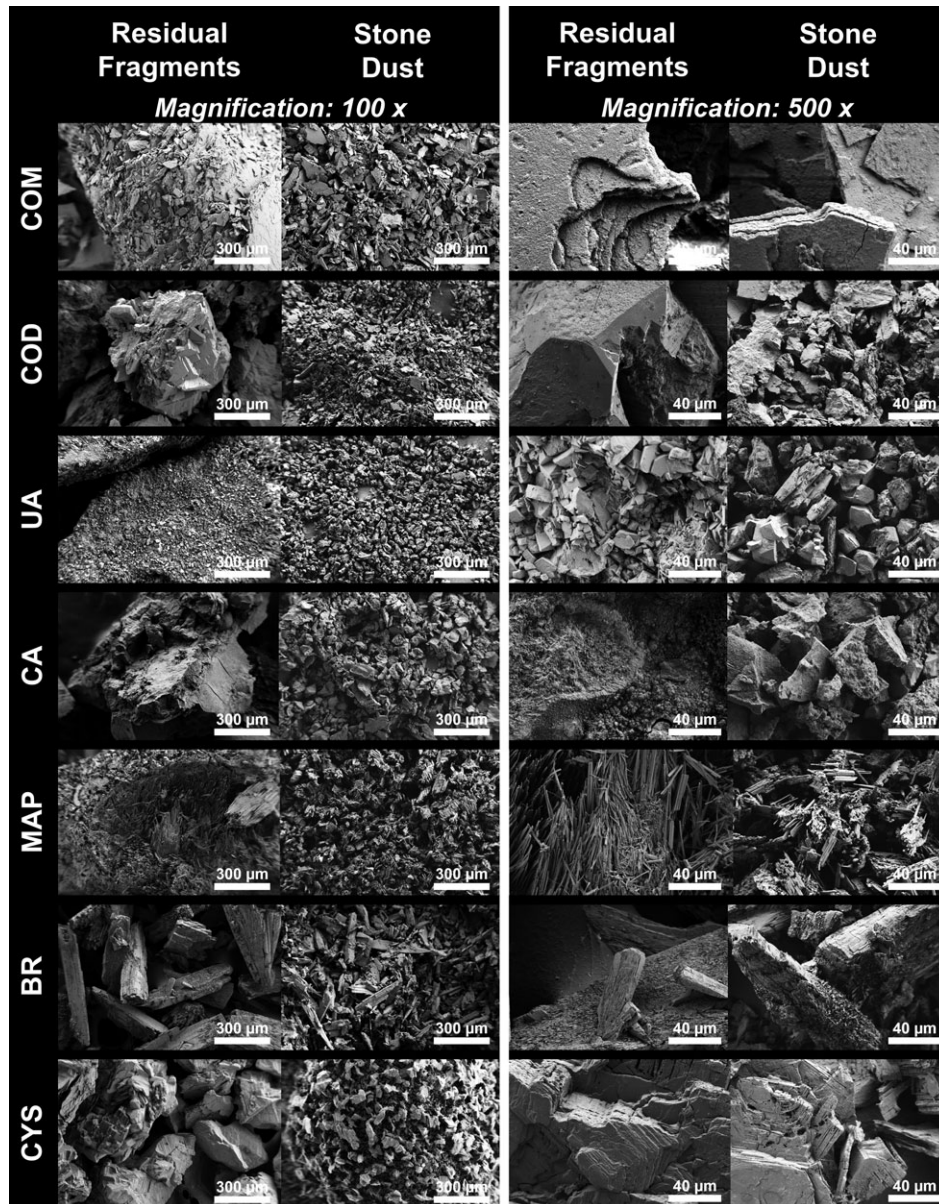
**FIGURE 3** Morphological analysis by scanning electron microscopy. Each stone constituent was analyzed by SEM at magnifications of 100× and 500×. Low electron beam voltage (≤2 keV) was used and no sample coating or fixation was needed image acquisition
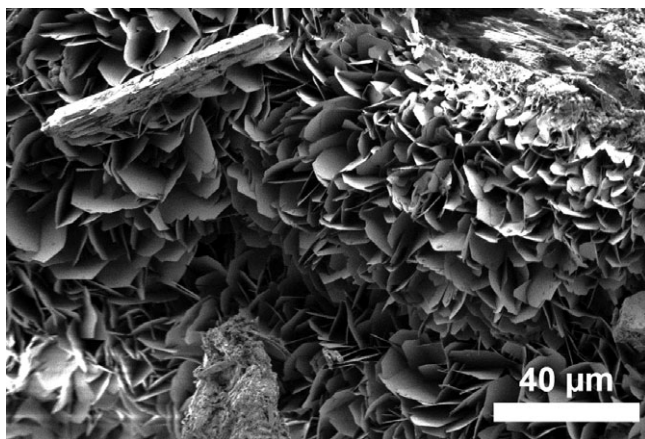


**FIGURE 4** Plate-like hydroxyapatite. SEM analyzes areas of hexagonal plate-like surfaces at the tip of BR baguettes after Moses lithotripsy

ammonium carbonate and magnesium carbonate as well as CYS to free sulfur and cysteine suggest that a photothermal effect of Holmium laser causes urinary stones to assume their more stable crystalline form [3, 4].

A limitation of this study was the lack of a clear definition of stone dust at the time the study was conducted. Various definitions can be found in literature, mostly describing fragments <1 mm which cannot be retrieved by stone baskets [21, 22]. In this study, a genuine methodology relying on the floating ability of particles was proposed for separation of RF from stone dust. The rationale for this separation method was the observation of spontaneous evacuation of stone dust during retrograde surgery in our clinical practice, which seemed to be related to the floating ability of particles using an irrigation pressure of 40 cm
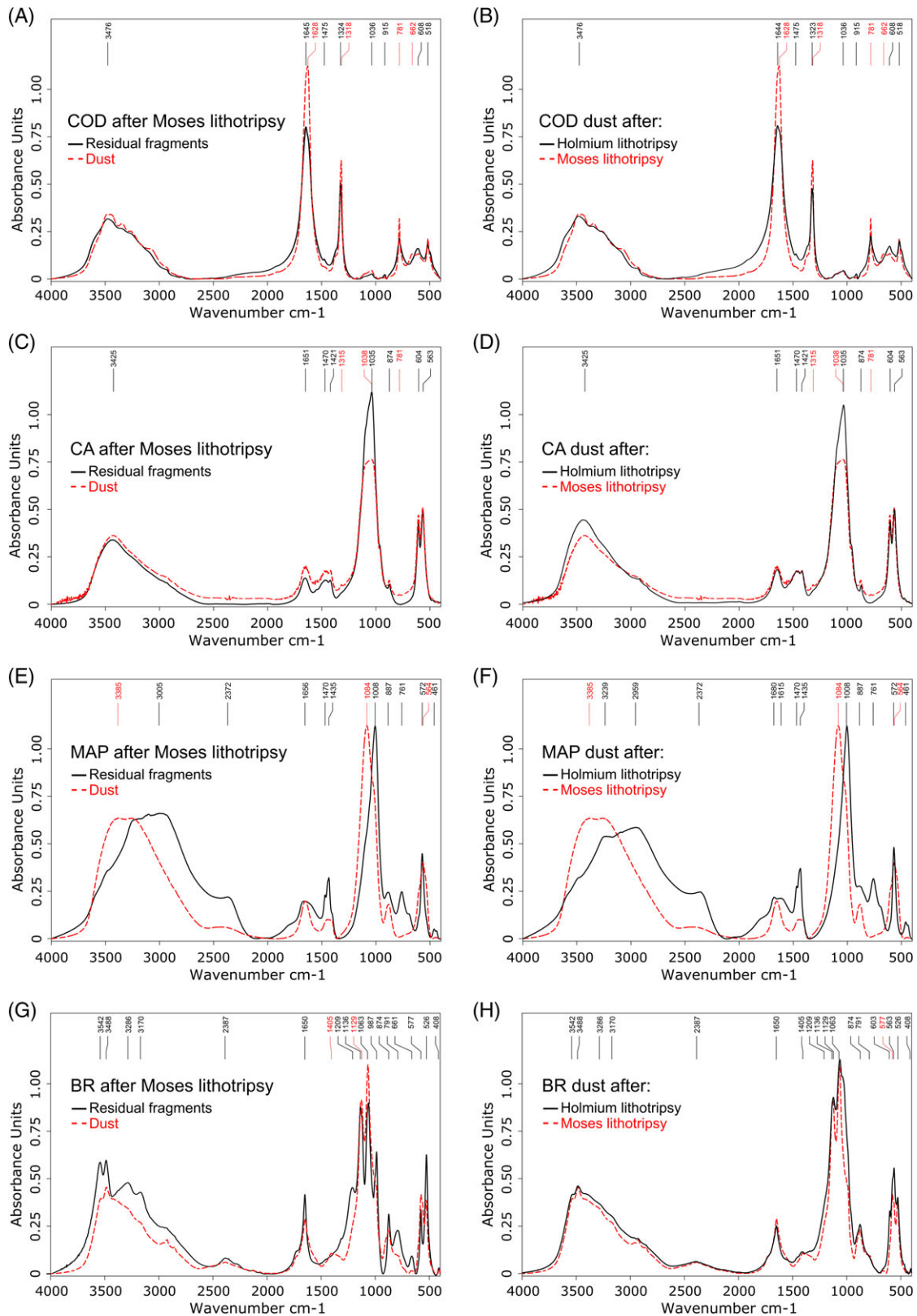
**FIGURE 5** Constitutional analysis by Fourier-transform infrared spectroscopy. Comparison between RF and stone dust revealed spectra changes for several constitutional stone types. A. Conversion from COD towards COM in dust after Moses lithotripsy. B, The conversion from COD towards COM in dust was more pronounced after Moses lithotripsy compared to conventional Holmium lithotripsy. C, Changes towards an amorphous phase in CA dust after Moses lithotripsy with flattening and displacement of the 1035 cm$^{-1}$ band. D, A spectral change of CA dust was only found after Moses lithotripsy, but not after conventional Holmium lithotripsy. E, Changes towards a differing and amorphous crystalline phase in MAP dust after Moses lithotripsy. F, A spectral change of MAP dust was only found after Moses lithotripsy, but not after conventional Holmium lithotripsy. G, Changes from BR towards CA after Moses lithotripsy. H, Spectral changes were found in CA dust both after Moses and conventional Holmium lithotripsy

H20 through the fURS working channel. We referred this phenomenon as the "snow globe effect". Further studies are warranted to verify the validity of this new separation method of stone disintegration products. Also, further studies shall evaluate whether other experimental settings such as altered laser parameters or various morphological stone subtypes (eg, Ia instead of Id) would impact on the present findings.

## 5 | CONCLUSIONS

Morpho-constitutional analysis of stone disintegration products reveals yet uncovered insight into the ablative effect of Holmium laser on urinary stones. Depending on major crystalline constituents, stone dust either conserves all attributes found in larger RF or shows changes in crystalline organization. Moses technology seems to produce more pronounced changes. These findings suggest a photothermal effect of Holmium laser on stones and shall be considered for future studies on laser lithotripsy, as stone dust may not adequately reflect crystalline organization of the stones before laser lithotripsy.

## AUTHOR BIOGRAPHIES

Please see Supporting Information online.

## ORCID

*Etienne X. Keller* https://orcid.org/0000-0003-1667-7609
*Vincent de Coninck* https://orcid.org/0000-0002-4983-5055
*Olivier Traxer* https://orcid.org/0000-0002-2459-3803

## REFERENCES

[1] S. Pierre, G. M. Preminger, *World J Urol* **2007**, *25*, 235.
[2] E. D. Jansen, T. G. van Leeuwen, M. Motamedi, C. Borst, A. J. Welch, *Lasers Surg Med* **1994**, *14*, 258.
[3] K. F. Chan, G. J. Vassar, T. J. Pfefer, J. M. H. Teichman, R. D. Glickman, S. T. Weintraub, A. J. Welch, *Lasers Surg Med* **1999**, *25*, 22.
[4] G. J. Vassar, K. F. Chan, J. M. H. Teichman, R. D. Glickman, S. T. Weintraub, T. J. Pfefer, A. J. Welch, *J Endourol* **1999**, *13*, 181.
[5] K. F. Chan, T. J. Pfefer, J. M. H. Teichman, A. J. Welch, *J Endourol* **2001**, *15*, 257.
[6] J. M. Isner, A. R. Lucas, *Br J Hosp Med* **1988**, *40*, 172.
[7] M. M. Elhilali, S. Badaan, A. Ibrahim, S. Andonian, *J Endourol* **2017**, *31*, 598.
[8] J. M. H. Teichman, G. J. Vassar, J. T. Bishoff, G. C. Bellman, *J Urol* **1998**, *159*, 17.
[9] A. H. Aldoukhi, W. W. Roberts, T. L. Hall, K. R. Ghani, *Front Surg* **2017**, *4*, 57.
[10] C. A. Dauw, L. Simeon, A. F. Alruwaily, F. Sanguedolce, J. M. Hollingsworth, W. W. Roberts, G. J. Faerber, J. S. Wolf Jr., K. R. Ghani, *J Endourol* **2015**, *29*, 1221.
[11] E. R. Ray, G. Rumsby, R. D. Smith, *BJU Int* **2016**, *118*, 618.
[12] M. Daudon, A. Dessombz, V. Frochot, E. Letavernier, J.-P. Haymann, P. Jungers, D. Bazin, *C R Chim* **2016**, *19*, 1470.
[13] J. E. Santiago, A. B. Hollander, S. D. Soni, R. E. Link, W. A. Mayer, *Curr Urol Rep* **2017**, *18*, 32.
[14] B. R. Matlaga, B. Chew, B. Eisner, M. Humphreys, B. Knudsen, A. Krambeck, D. Lange, M. Lipkin, N. L. Miller, M. Monga, V. Pais, R. L. Sur, O. Shah, *J Endourol* **2018**, *32*, 1.
[15] D. Bazin, *Ann Biol Clin* **2015**, *73*, 517.
[16] M. Daudon, P. Jungers, in *Urolithiasis: Basic Science and Clinical Practice* (Eds: T. H. Talati, A. D. M. JJ, Z. Ye), Springer, London, UK **2012**, p. 113.
[17] J. Cloutier, L. Villa, O. Traxer, M. Daudon, *World J Urol* **2015**, *33*, 157.
[18] L. Estepa, M. Daudon, *Biospectroscopy* **1997**, *3*, 347.
[19] S. A. Schafer, F. M. Durville, B. Jassemnejad, K. E. Bartels, R. C. Powell, *IEEE Trans Biomed Eng* **1994**, *41*, 276.
[20] G. J. Vassar, J. M. H. Teichman, R. D. Glickman, *J Urol* **1998**, *160*, 471.
[21] J. Sea, L. M. Jonat, B. H. Chew, J. Qiu, B. Wang, T. Hoopman, T. Milner, J. M. H. Teichman, *J Urol* **2012**, *187*, 914.
[22] M. Kang, H. Son, H. Jeong, M. C. Cho, S. Y. Cho, *World J Urol* **2016**, *34*, 1591.